Transaction

Structure and Mechanical Properties of Poly(trimethylene terephthalate) Fibers Obtained by CO_2 Laser Drawing and a Secondary Contact Heater Drawing

Young-Ah Kang[*1], *Kyoung-Hou Kim*[*2], *Xin Zhao*[*3], *Yang Hun Lee*[*4], *Toshifumi Ikaga*[*3], *and Yutaka Ohkoshi*[*3,#]

[*1] Research Institute of Human Ecology, Dong-A University, Korea
[*2] Textile & Consumer Goods Examination Division, Korean Intellectual Property Office, Korea
[*3] Faculty of Textile Science and Technology, Shinshu University, Japan
[*4] Department of Textile Industry, Dong-A University, Korea

Abstract: CO_2 laser drawing heats a running fiber homogeneously and rapidly without contact by laser irradiation and develops a necking in a fixed location. As-spun fibers of bio- and chemo-based poly(trimethylene terephthalate) (PTT) were drawn to draw ratio (DR) of 3.5-5.5 and 3.5-4.8 by CO_2 laser-heated drawing, respectively, which was taken as the first drawing. Secondarily the first-drawn fibers were drawn to total draw ratio (TDR) as high as possible by direct contact heater drawing of 150°C, which attained TDR 5.60-5.70 and 5.40-5.46 for bio- and chemo-based PTT fibers, respectively. Drawing stress in situ measured in the two-steps drawing increased roughly proportional to draw ratio, and for bio-based PTT was higher than for chemo-based one when compared at the same DR and TDR. We investigated in this study the structure and mechanical properties of the drawn PTT fibers by wide angle X-ray diffraction (WAXD), birefringence, thermo-mechanical property, and tensile property. The typical WAXD pattern of PTT crystal was observed with orientation-induced crystallization by the two-steps drawing. But, the meridional reflections become blurred and their intensities decrease with increasing draw ratio and by the second drawing. The transverse crystallite sizes, along the normal direction of (010) plane, increased transversely but the longitudinal sizes, along the normal direction of (002) plane decreased longitudinally as draw ratio increased for chemo-based PTT, whereas for bio-based PTT, the crystallite size change with draw ratio was the same trend with the chemo-based by the first drawing but the crystallite became much smaller transversely and longitudinally by the second drawing. By the azimuthal intensity profile, the crystal orientation factor obtained from (010) plane increased, while that from (002) plane decreased with the total draw ratio. The birefringence was a constant value 0.07 with no dependence on draw ratio by two steps drawing, which is over twice a reported intrinsic birefringence of PTT crystal, 0.029 [12]. Also, Young's modulus held an almost constant value of 2.3-2.6 GPa by the two stages drawing, which is very closed to 2.59 GPa, the theoretical modulus of PTT crystal.

(Received 27 February, 2013 ; Accepted 9 April, 2013)

1. Introduction

Poly(trimethylene terephthalate) (PTT) is an aromatic polyester with an odd-numbered methylene units, but there have been few studies for PTT so far compared to the even-numbered poly(ethylene terephthalate) (PET) and poly(butylene terephthalate) (PBT) with two and four methylene units, respectively. Because the commercial production of PTT was not realized until the mid-1990s, when the manufacturing cost of 1,3-propandiol (PDO) dropped drastically, although the polymerization of PTT was first reported by Whinfield and Dickson of Caligo Printing Ink Co. in 1941. Recently, a biologically-produced PDO was derived from microorganism metabolism of plant-derived sugars composed of carbon of atmospheric origin, and not composed of fossil-fuel carbon [1], and a bio-based PTT polymerized with the bio-PDO™ was produced as a fossil-fuel substitute.

PTT has some unique properties. Ward and his colleagues [2, 3] studied systematically on PTT fiber properties and deformation and found PTT to have a very good tensile elastic recovery. It ranked in a descending order PTT>PBT>PET. The fiber period along c-axis for PTT fiber measured as a function of strain when in situ deformed in a wide angle X-ray diffractometer was found to increase in direct proportion to the applied strain up to 4% and it was reversible below a critical strain. The reversible crystal deformation was attributed to the

corresponding author

flexible part consisting of a three-methylene group with an energetically favored trans-gauche-gauche-trans conformation. This helical conformation for PTT caused low crystal modulus, and indeed, Nakamae et al. [4] found PTT to have a very low crystal modulus of 2.59 GPa compared to 107 GPa of PET [5].

The crystal structure of PTT was determined by some researchers for samples prepared under various conditions [6-9]. According to Poulin-Dandurand [6], the unit cell of PTT is triclinic with parameter : a= 0.464 nm, b= 0.627 nm, c= 1.864 nm, α= 98.4°, β= 93.0°, and γ= 111.1°, with crystalline density being 1.387 g/cm^3, and with amorphous density being 1.299 g/cm^3 [10]. Semicrystalline PTT samples have been subjected to a detailed thermal analysis [11, 12], where glass transition and typical onset temperatures of melting endotherm were reported to be 45 and 228°C, respectively. For 100% crystalline PTT, the heat of fusion is estimated to be 30± 2 kJ/mol.

Our research group has in-situ studied on the fiber structure development mechanism in a continuous neck-drawing of PTT [13]. Necking occurred when fiber temperature increased to about 90°C by laser irradiation, and the orientation-induced crystallization was developed initially at an elapsed time of 0.415 ms after necking in the neck-drawing. With elapsed time, the interplanar spacing of (002) plane decreased gradually due to transformation of the initial all-trans conformation into trans-gauche-gauche-trans conformation, and ultimately the PTT molecular chain adopted favorably the trans-gauche-gauche-trans conformation.

In this article we report structural changes and improved mechanical properties of chemo- and bio-based PTT fibers by two-steps drawing, i.e., the first neck-drawing using a CO_2 laser irradiation and the second drawing using a direct contact heater. The structural changes and mechanical properties were studied by birefringence, wide angle X-ray diffraction (WAXD) and tensile properties.

2. Experimental

2.1. Samples and melt spinning

Two types of PTT polymers, which were polymerized with chemically and biologically-derived PDO, were used in this study. They were referred to chemo-based PTT (Shell Chemicals, IV 0.92 dl/g) and bio-based PTT (DuPont, IV 0.93 dl/g) respectively. The polymers were melt-spun with a mass flow rate of 1.725 g/min and a take-up speed of 170 m/min at 260°C. The produced fibers were 101±7 μm in diameter and exhibited an amorphous halo in a WAXD image.

2.2. CO_2 laser absorption coefficient

The absorption coefficient of CO_2 laser for PTT was characterized by means of a Fourier transform infrared (FT-IR) spectrometer. The wavelength used for the CO_2 laser is 10.6 μm, corresponding to 943 cm^{-1}. The infrared absorbance at the wavenumber was plotted against various film thicknesses, and the absorption coefficient was obtained by the gradient of approximation line. The absorption coefficients for chemo-based PTT has been reported to be 3.42×10^4 m^{-1} [13], and the obtained absorption coefficient for bio-based PTT was found to be 3.53×10^4 m^{-1}. The absorption coefficient shows that the fiber having above mentioned diameter can be heated almost homogeneously by the 3-directional laser irradiation as noted follows [20].

2.3. Drawings

The as-spun PTT fibers were firstly drawn by a CO_2 laser-heated drawing system. In the first drawing, the running fiber was heated by the irradiation of 3-directional CO_2 laser beam generated by a PIN-20S laser source manufactured by Onizuka Co. Ltd. The laser source has a rated power 20±1 W and a laser beam diameter of 5 mm. The fibers were drawn to draw ratios (DR) of 3.5, 4.0, 4.5, and 4.8 for the chemo-based PTT and 3.5, 4.0, 4.5, 5.0, and 5.5 for the bio-based by the first- drawing. Then, the firstly drawn fibers were secondarily drawn using a direct contact heater drawing system to total draw ratios (TDR) of 5.6-5.7 and 5.40-5.46 for the bio- and the chemo-based, respectively. Drawing conditions of the first and second drawings for two types of PTT fiber were presented in Table 1. The fiber feed speeds were 4.0 m/min and 2.0 m/min for the first and second drawing. The laser power for the first drawing was decided so as to be drawn most stably, and the maximum draw ratio for each drawing was decided so as to be stable over 5 minutes. An applied laser power was measured using a PW-250 powermeter of SYNRAD Co. Ltd. Drawing tension during the two-steps drawing was measured by EIKO HS-1500S tension meter. The measured data was collected by PC every 100 ms after A/D converting by KEYENCE NR-2000 data sampler. The drawing stress was obtained from the averaged drawing tension divided by the cross-sectional area obtained from the diameter of drawn fiber.

2.4. Refraction index and birefringence

Refractive indices along the parallel ($n_{//}$) and perpendicular ($n_{\perp}$) to the fiber axis were measured by the interference microscope of Carl-Zeiss Jena. Mixture of

Table 1 Drawing conditions.

Polymer Types	The 1st drawing		The 2nd drawing		Total Draw Ratio
	Draw Ratio	Laser Power (W)	Draw Ratio	Heater Temp. (°C)	
Bio–based	3.5	2.2	1.60	150	5.60
	4.0	2.4	1.43	150	5.70
	4.5	2.4	1.27	150	5.70
	5.0	2.7	1.14	150	5.70
	5.5	3.0	1.04	150	5.70
Chemo–based	3.5	1.7	1.56	150	5.46
	4.0	2.5	1.35	150	5.40
	4.5	3.1	1.20	150	5.40
	4.8	3.5	1.13	150	5.42

methylene iodide and tricresyl phosphate was used for the immersion oil whose refractive indices were measured by ATAGO Abbe refractometer 4T. The birefringence Δn and the average refractive index $\bar{n}$ were calculated by Eq. (1) and Eq. (2). Lorentz-Lorenz density was also obtained by Eq. (3). Here the N is the Avogadro's number, d is the density of fiber, P is the molar polarisability, and M is the molecular weight.

$$\Delta n = n_{//} - n_{\perp} \quad (1)$$

$$\bar{n} = \frac{n_{//} + 2n_{\perp}}{3} \quad (2)$$

$$\frac{\bar{n}^2 - 1}{\bar{n}^2 + 2} = \frac{\pi N d P}{3M} \quad (3)$$

2.5. X-ray diffraction analysis

Wide angle X-ray diffraction (WAXD) patterns and intensity profiles were obtained with Rigaku RU200B X-ray generator with the light source of Cu-K_α (0.15418 nm). The imaging plate of 1150 × 1150 pixels were used to get the WAXD patterns, and the intensity profiles along the equatorial, meridional, and azimuthal directions for (010) and (002) diffractions were taken with the goniometer PMG-RAN215505. The slit width, scan speed, and sampling step were 0.5°, 2°/min, and 0.02° for diffraction angle directions, and 0.5°, 20°/min, and 0.1° for azimuthal angle directions, respectively.

2.6. Thermo-mechanical properties

Thermal shrinkage with temperature was measured using an EXTRA 6000 TMA (thermo-mechanical analyzer) of SII Nanotechnology Co. A 5 mm long fiber was heated from room temperature to 300°C with the heating rate of 5 K/min under the constant stress and fixed length conditions. Percent thermal shrinkage, thermal shrinkage stress, the maximum shrinkage temperature, and the maximum shrinkage stress temperature were obtained by the measurement.

2.7. Mechanical properties

Mechanical properties of drawn PTT fibers were measured with a Shimazu Autograph AGS-X tensile tester equipped 50 N load-cell at room temperature. All tests were performed using a gauge length of 40 mm and a constant cross-head speed of 100%/min. An average of 10 individual tensile tests was reported for each sample. For a stretch cycle test, a 100 mm long filament was stretched into an elongation of 20% at a cross-head speed of 100%/min, and the cross-head was then immediately returned to an initial load of 0.05 N. The elastic recovery (ER) was calculated according to Eq. (4), where L_0 is the original length of filament, L is the irreversible length of the filament after the cross-head was returned.

$$\mathrm{ER} = \frac{(L_0 - L)}{L_0} \times 100 \quad (4)$$

3. Results and discussion

3.1. Necking

The morphological change around the necking

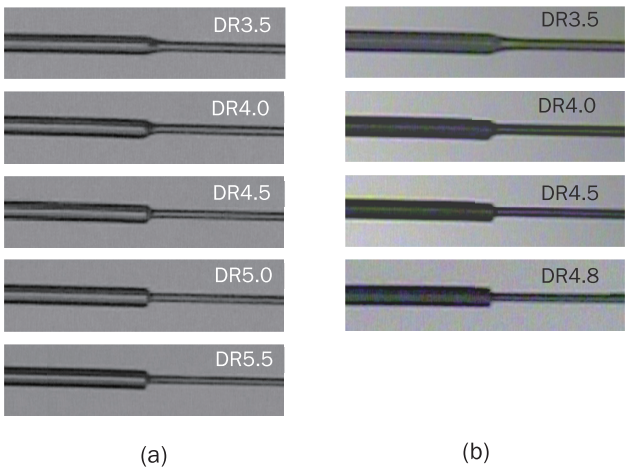

Fig. 1 Necking shape captured in the first-step drawing for bio-based (a) and chemo-based (b) PTT fibers. Draw ratios were noted in the respective figures.

developed by the CO_2 laser irradiation in the first drawing of bio- and chemo-based PTT fibers was monitored by a CCD camera, and captured images are shown in Fig. 1. The diameter decline by the necking grows steeper as draw ratio increases. Moreover, bio-based PTT fiber was to be steadily drawn to higher draw ratio than chemo-based one. But there is no difference in intrinsic viscosity of both raw PTT samples, indicating no difference in average molecular weight. It has been reported the higher purity propandiol could be made by the bio-based process than chemo-based process and result in the bio-based PTT polymer having the lower oligomer contents [1]. Thus, the drawability to higher draw ratio for bio-based PTT is probably attributed by a narrow molecular weight distribution. Also this better drawability for bio-based PTT can result in a good mechanical property.

3.2. Drawing stress

Drawing stress was in situ measured in the first and the second drawing, and is shown with draw ratio in Fig. 2. Drawing stress monotonically increases with draw ratio by the first drawing for two types of PTT fiber, and also largely increases by the second drawing. The drawing stresses for bio-based PTT are higher than those for chemo-based one when compared them at the same draw ratio and the second drawing.

3.3. Structure change

Structure changes of PTT fibers by the first and second drawings are studied through WAXD patterns, which are shown in Figs. 3 and 4, in which total crystal reflections for PTT are identified. Draw ratios are noted

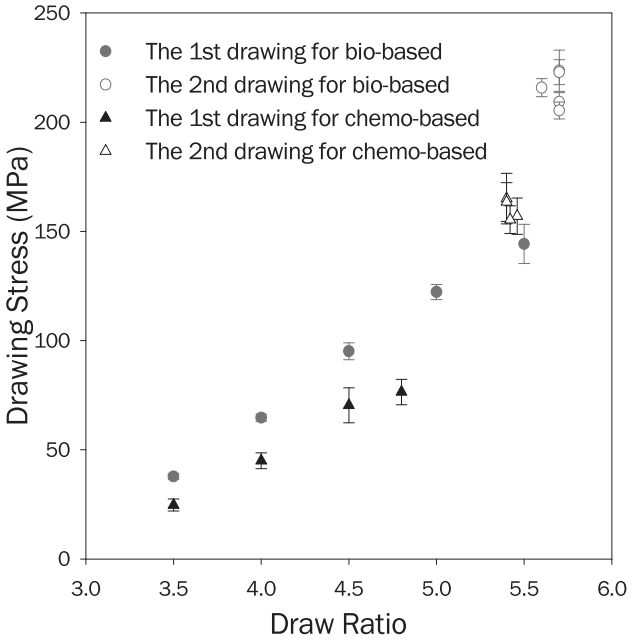

Fig. 2 Drawing stress with draw ratio in the first- and the second-step drawings for bio- and chemo-based PTT fibers.

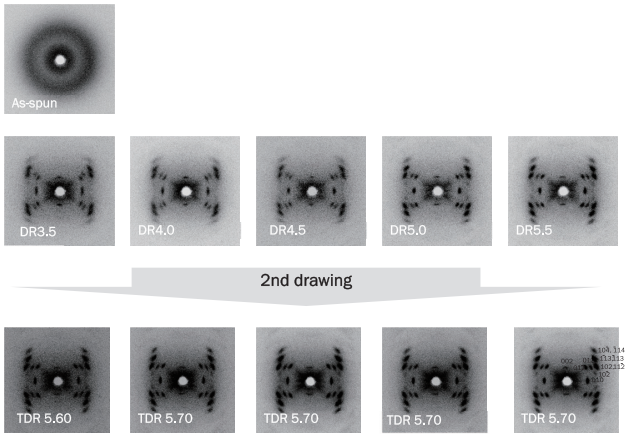

Fig. 3 WAXD images of bio-based PTT fibers drawn by the first- and the second-step drawings. The total draw ratios were noted in the respective figures.

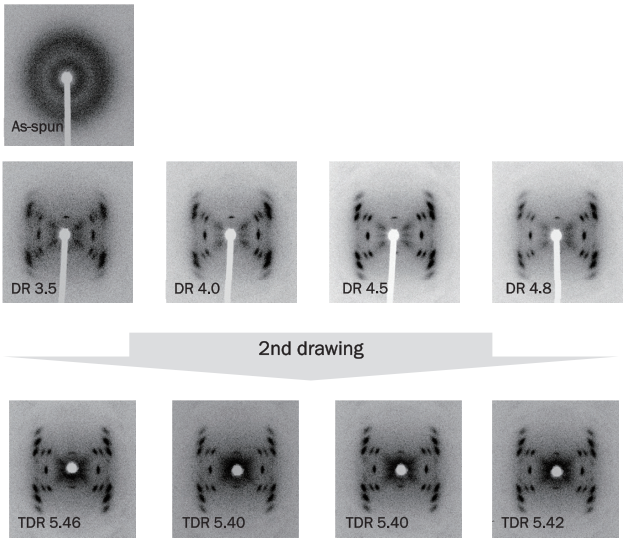

Fig. 4 WAXD images of chemo-based PTT fibers drawn by the first- and the second-step drawings. The total draw ratios were noted in the respective figures.

inside the figures. As-spun fibers show halo, indicating low oriented and amorphous state. The amorphous halo is concentrated to crystal reflections by the first drawing. There are one reflection of (010) plane on the equator, one reflection of (002) on the meridian, and other six reflections off the equator. All of the crystal reflection intensities increase with orientation-induced crystallization by the two-steps drawing. But, the meridional reflections become blurred and their intensities decrease with increasing draw ratio by the second drawing.

The intensity profiles of (010) and (002) reflections were fitted by the Gaussian function (Eq. (5)), which determined the position $2\theta_0$ and full width at half maximum β, and the crystallites sizes were estimated by Scherer's formula (Eq. (6)) with the constant K of 0.918.

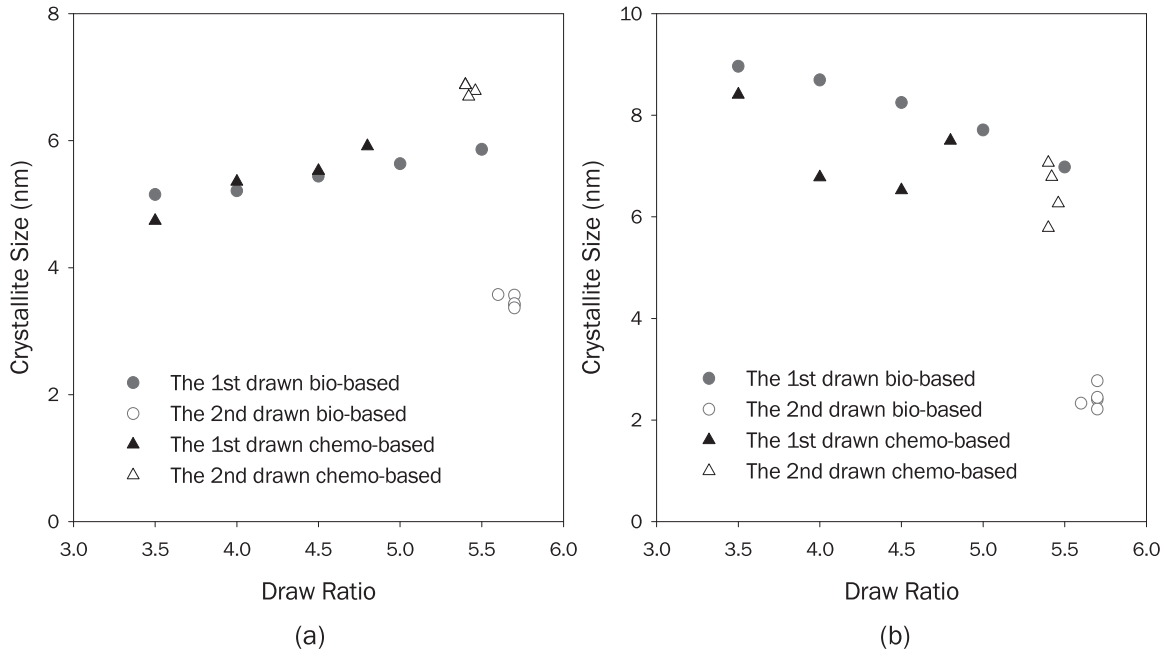

Fig. 5 Crystallite sizes along the normal direction of (010) (a) and (002) (b) planes with draw ratio.

The crystallite sizes along the normal direction of (010) and (002) planes with draw ratio are shown in Figs. 5 (a) and (b), respectively. For bio-based PTT, the crystallite size along the normal direction of (010) plane increases with draw ratio of the first drawing but decreases largely by the second drawing, whereas the crystallite size of (002) shrinks gradually with increasing draw ratio and reduces significantly by the second drawing. On the other hand, for chemo-based PTT, the (010) crystallite size increases gradually with draw ratio by two-steps drawing while the (002) crystallite size decreases with increasing draw ratio. Accordingly, for chemo-based PTT, the crystallite sizes increased transversely but decreased longitudinally as draw ratio increased, whereas for bio-based PTT, the crystallite size change with draw ratio was the same trend with the chemo-based by the first drawing but the crystallite became much smaller transversely and longitudinally by the second drawing. We have reported that the longitudinal structure was developed prior to the transverse structure by the necking [13]. The longitudinal structure, supports the fiber longitudinally, may play an important role in determining the mechanical properties.

$$I(2\theta)=I_o\exp\left(-4\ln 2\cdot\left(\frac{2\theta-2\theta_o}{\beta}\right)^2\right) \quad (5)$$

$$L_{hkl}=\frac{K\lambda}{\beta\cos\theta} \quad (6)$$

The crystallinity index obtained by the integral intensity of (010) diffraction in the total equatorial diffraction angles from 5 to 40° is shown in Fig. 6. The crystallinity index increases gradually with draw ratio through the two-steps drawing. Because the crystallinity index was obtained by the equatorial integration, it can be influenced by the crystal orientation. But as shown below, the crystal orientation factor of (010), over 0.94, is sufficiently high for the drawn fibers. In addition, the increasing trend of crystallinity index was consistent with that of Lorentz density as shown below. Thus, it can be said that the number of crystallite increase with the draw ratio and by the two-steps drawing.

Azimuthal intensity profiles were also fitted by the Gaussian function, and the crystal orientation factor (f)

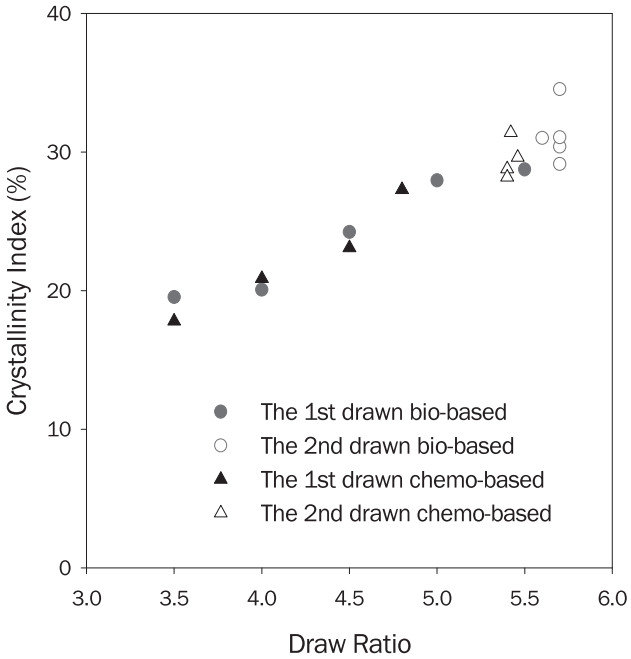

Fig. 6 Crystallinity index obtained by the integral intensity of (010) diffraction in the total equatorial diffraction angles from 5 to 40°.

was calculated by Eq. (7) with the integration of fitted curves along the azimuthal angles from 0° to 360°. The calculated orientation factors are shown in Figs. 7 (a) and (b). The crystal orientation factor obtained from the (010) plane increases with draw ratio and is saturated at about 0.97, while the orientation factor from the (002) plane decreases and is saturated at about 0.90. The difference on crystal orientation factors and their trend between two directions should be caused by the tilting of orientation axis. Because the crystal form of PTT crystal is triclinic, not only crystal orientation factor but also the direction of orientation axis can be changed by the drawing. The opposite trend of (010) and (002) plane orientations can be explained that the c^*-axis orientation for the low draw ratio case was changed to the c-axis orientation for the high draw ratio case.

$$f=\frac{3\langle\cos^2\phi\rangle-1}{2} \tag{7}$$

On the other hand, total chain orientation by the first and second drawing is measured by birefringence calculated from the refractive indices parallel and normal to fiber axis with draw ratio for bio- and chemo-based PTT are shown in Figs. 8 (a) and (b), respectively. As-

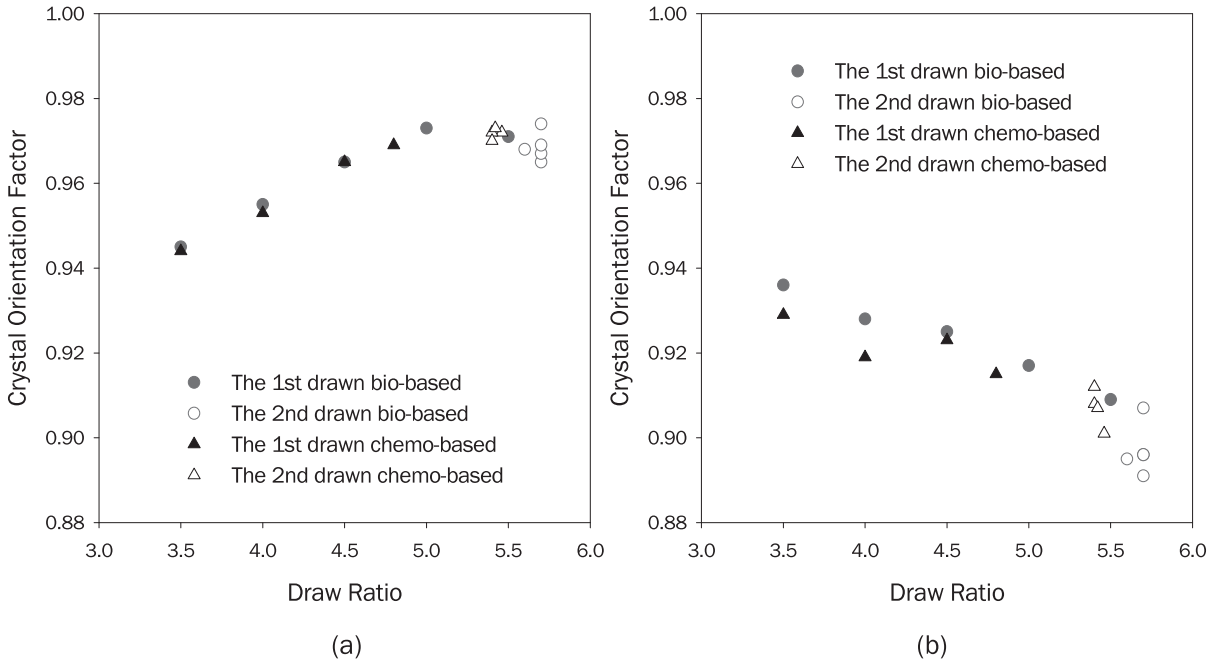

Fig. 7 Crystal orientation factors obtained from azimuthal intensity profiles of (010) (a) and (002) (b) planes.

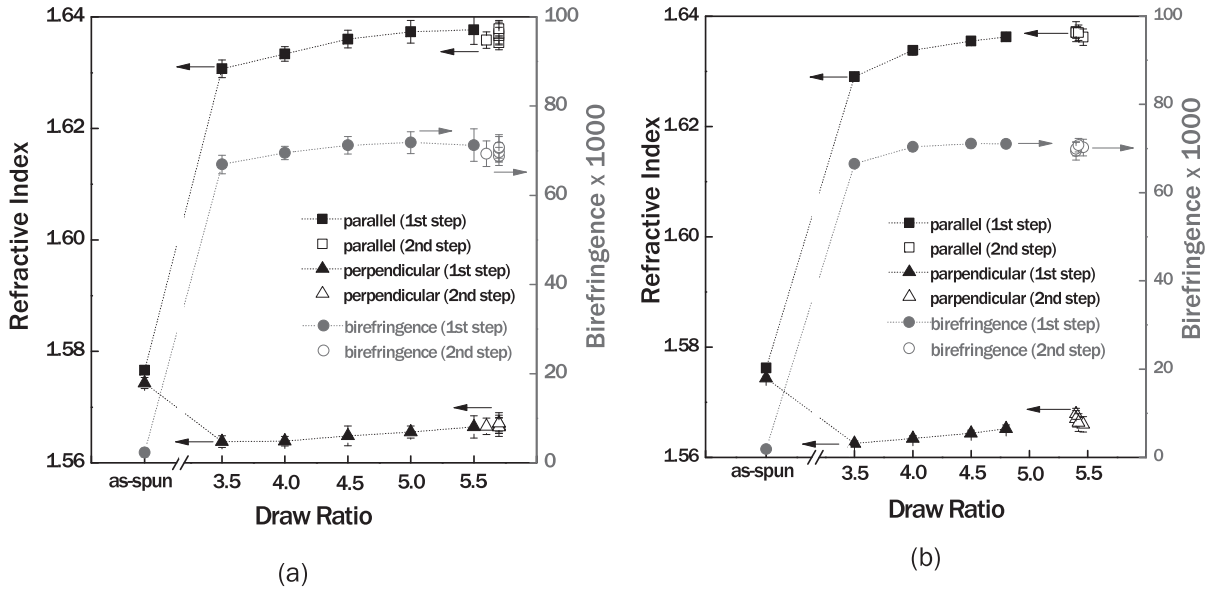

Fig. 8 Birefringence and refractive indices along parallel and perpendicular direction to fiber axis with draw ratio for bio- (a) and chemo-based (b) PTT fibers.

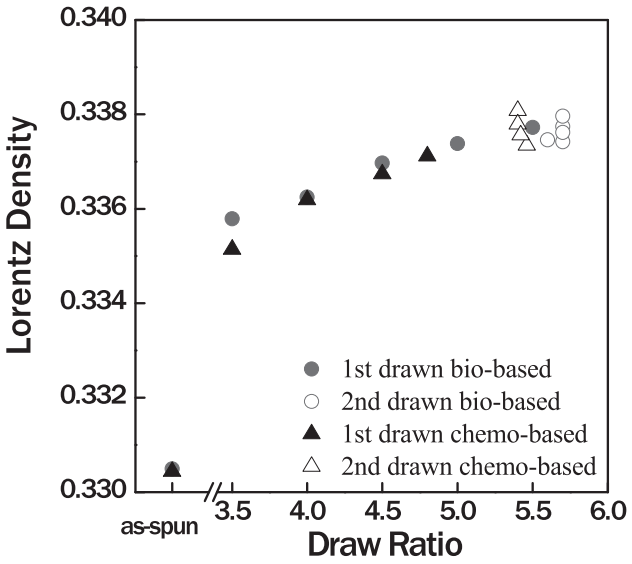

Fig. 9 Lorentz densities with draw ratio.

spun fibers for bio- and chemo-based PTT show almost zero birefringence. By the first neck-drawing, the refractive indices much increase along parallel direction to the fiber axis while decrease along normal direction, and it causes the increase of birefringence. But, as draw ratio increases, the refractive indices along both parallel and normal directions increase for both types of PTT, which leads an almost saturated birefringence of 0.07. The saturated birefringence value of 0.07 is over twice a reported intrinsic birefringence value of PTT crystal, 0.029 [12], but is still less than the intrinsic birefringence 0.22 of chemically similar PET crystal [15]. Far lower intrinsic birefringence value of PTT crystal than PET is caused by the difference of methylene chain conformation, trans-gauche-gauche-trans. Ultimately, it can be explained that the two-steps drawing not only increases the amorphous chain orientation but also forms extended amorphous chain to indicate higher birefringence than the chain in crystal.

Lorentz density calculated from Eq. (3) is shown in Fig.9. The Lorentz density increases with draw ratio by the two-steps drawing. It well corresponds to the crystallinity index change of Fig. 6. Thus, the crystal fraction increases with the orientation-induced crystallization.

3.4. Thermo-mechanical properties

For the constant stress conditions, the length of drawn fiber decreases with increasing temperature and takthes maximum at a certain temperature, and the stress also takes maximum for the fixed length conditions. From the data of TMA measurements, percent maximum shrinkage, maximum shrinkage temperature, maximum shrinkage stress, and maximum shrinkage stress temperature were estimated and presented in Table 2. The fiber length shrinkage, increasing with temperature, takes the maximum at temperatures 6-9 K lower than melting temperature for both types of PTT, and it indicates the length change could be caused by a disorientation of oriented amorphous chains. The maximum shrinkage increases with draw ratio by the first drawing but

Table 2 Thermo-mechanical properties.

Polymer types	Drawings	Draw ratio /Total draw ratio	Max. shrinkage		Max. shrinkage stress	
			temp. (°C)	Value (%)	temp. (°C)	Value (MPa)
Bio-based	The 1st drawing	3.50	218.8	11.2	139.0	14.3
		4.00	217.5	14.8	153.0	20.7
		4.50	218.9	16.2	161.0	24.1
		5.00	220.5	17.3	171.0	32.8
		5.50	220.4	17.3	178.0	31.4
	The 2nd drawing	5.60 (3.5)	219.5	14.0	191.4	28.5
		5.70 (4.0)	218.6	13.6	191.5	27.9
		5.70 (4.5)	219.1	13.9	192.6	28.8
		5.70 (5.0)	220.0	15.4	190.4	33.4
		5.70 (5.5)	221.9	15.7	189.6	35.2
Chemo-based	The 1st drawing	3.50	217.1	12.6	142.5	13.5
		4.00	216.8	16.9	148.7	28.2
		4.50	217.8	18.3	162.1	32.1
		4.80	218.7	18.9	187.0	29.1
	The 2nd drawing	5.46 (3.5)	219.2	17.7	186.1	37.1
		5.40 (4.0)	216.5	17.6	186.5	34.2
		5.40 (4.5)	215.3	17.5	187.5	34.6
		5.42 (4.8)	216.4	17.9	188.8	35.7

* Values in bracket beside total draw ratio are draw ratio of the first-step drawing.

decreases somewhat by the second drawing. It can be elucidated that the amorphous chain orientation increases with draw ratio by the first drawing and then the crystallinity increase with heat-setting effect by the second drawing. And the length changes by thermal shrinkage are found to be larger for chemo-based PTT than for bio-based one. On the other hand, the stress change imposed by length shrinkage underwent an increase to the maximum and a decrease with temperature. The maximum shrinkage stress temperature increases with draw ratio and by the second drawing, and particularly shows a large increase by the second drawing for bio-based PTT.

3.5. Mechanical properties

Averaged Young's modulus, tensile strength, and elongation at break from stress-strain curves are presented in Table 3. Young's modulus by the drawings showed almost saturated value of 2.3-2.6 GPa. Tensile strength increased with draw ratio of the first drawing and by the second drawing, and notes the maximum value of 683 MPa (5.1cN/dtex) for bio-based fiber and 548 MPa (4.1cN/dtex) for chemo-based fiber. The increase of tensile strength seems to be related to the increase of amorphous orientation as shown before. Elongation decreased with draw ratio of the first drawing and by the second drawing, but it kept over 40% for the fiber indicating the maximum tensile strength. It is a noteworthy that the high-toughness PTT fiber which has both over 5 cN/dtex strength and over 40% elongation can be made by the first laser-heated drawing as well as the two-steps drawing in this study. The strength and elongation of PTT fibers are reported 3 cN/dtex and 50% by high-speed spinning [16, 17], 2.2 cN/dtex by zone-drawing [18], 3.7-5.4 cN/dtex and 22-31% by high-molecular weight PTT [19, 20]. The values obtained in this study are also higher than these reported values. The bio-based PTT fiber showed in particular the higher maximum strength than the chemo-based one. The higher draw ratio under the higher drawing stress should results the higher fiber strength.

Young's modulus of fiber increases by the drawings in general, but it held almost constant value of 2.3-2.6 GPa in this study, showing no dependence on draw ratio of the two stages drawing. This value is very close to 2.59 GPa [4], the theoretical modulus of PTT crystal. Very low theoretical modulus value of crystal can be explained by the unique chain conformation of PTT, that is, large helical conformation. The low crystal modulus should restrict the Young's modulus of drawn fiber in spite of the increase of crystallinity and molecular orientation in amorphous phase with the increase of draw ratio and by the second drawing.

Typical stress-strain curves with the respective draw ratio for both bio- and chemo-based drawn PTT fiber are shown Figs. 10 (a) and (b), respectively. All stress-strain curves show characteristically two yielding points. It is considered that the two-yielding phenomenon is probably due to a flexible PTT chain having a large helical conformation deform like a spring. The two yielding points appear around elongations of 5% and 20-30%. The second yielding revealed at high-elongation increases in both stress and strain with draw ratio and by the two-steps

Table 3 Mechanical properties.

Polymer types	Drawings	Draw ratio /Total draw ratio	Tensile strength (MPa)	Elongation (%)	Young's modulus (GPa)
Bio-based	The 1st drawing	3.5	415 ± 33	84 ± 10	2.48 ± 0.05
		4.0	469 ± 18	63 ± 3	2.49 ± 0.04
		4.5	555 ± 26	57 ± 3	2.51 ± 0.07
		5.0	619 ± 29	48 ± 3	2.55 ± 0.03
		5.5	664 ± 52	42 ± 3	2.53 ± 0.03
	The 2nd drawing	5.60 (3.5)	652 ± 21	56 ± 4	2.55 ± 0.01
		5.70 (4.0)	659 ± 26	51 ± 4	2.55 ± 0.01
		5.70 (4.5)	645 ± 22	51 ± 4	2.55 ± 0.02
		5.70 (5.0)	667 ± 15	48 ± 4	2.54 ± 0.02
		5.70 (5.5)	683 ± 37	45 ± 5	2.53 ± 0.04
Chemo-based	The 1st drawing	3.5	363 ± 13	86 ± 8	2.30 ± 0.10
		4.0	400 ± 13	65 ± 4	2.30 ± 0.10
		4.5	452 ± 15	52 ± 3	2.40 ± 0.10
		4.8	487 ± 12	43 ± 2	2.40 ± 0.10
	The 2nd drawing	5.46 (3.5)	548 ± 33	46 ± 5	2.40 ± 0.10
		5.40 (4.0)	516 ± 15	46 ± 2	2.40 ± 0.10
		5.40 (4.5)	525 ± 17	44 ± 4	2.50 ± 0.10
		5.42 (4.8)	516 ± 32	43 ± 4	2.40 ± 0.10

* Values in bracket beside total draw ratio are draw ratio of the first-step drawing.

drawing and particularly by the second drawing it exceed an elongation of 20%. It is expected that the reversible elasticity of PTT fibers below the second yielding could be almost maintained.

Thus, we measured stress-elongation curves in ten reversible-stretch cycles to an elongation of 20% for the first and second drawn both bio- and chemo-based PTT fibers, which showed hysteresis loops by immediate elastic recovery as presented in Figs. 11 (a) and (b). All drawn PTT samples show slight hysteresis loop in which

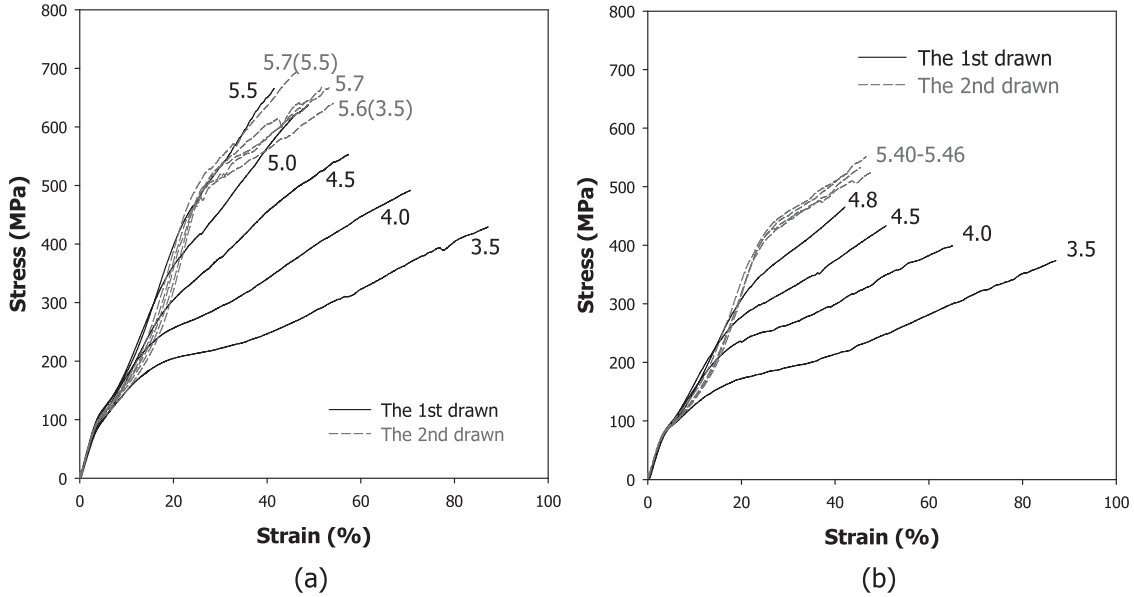

Fig. 10 Typical stress-strain curves for bio- (a) and chemo-based (b) drawn PTT fiber. Draw ratios were noted inside figures.

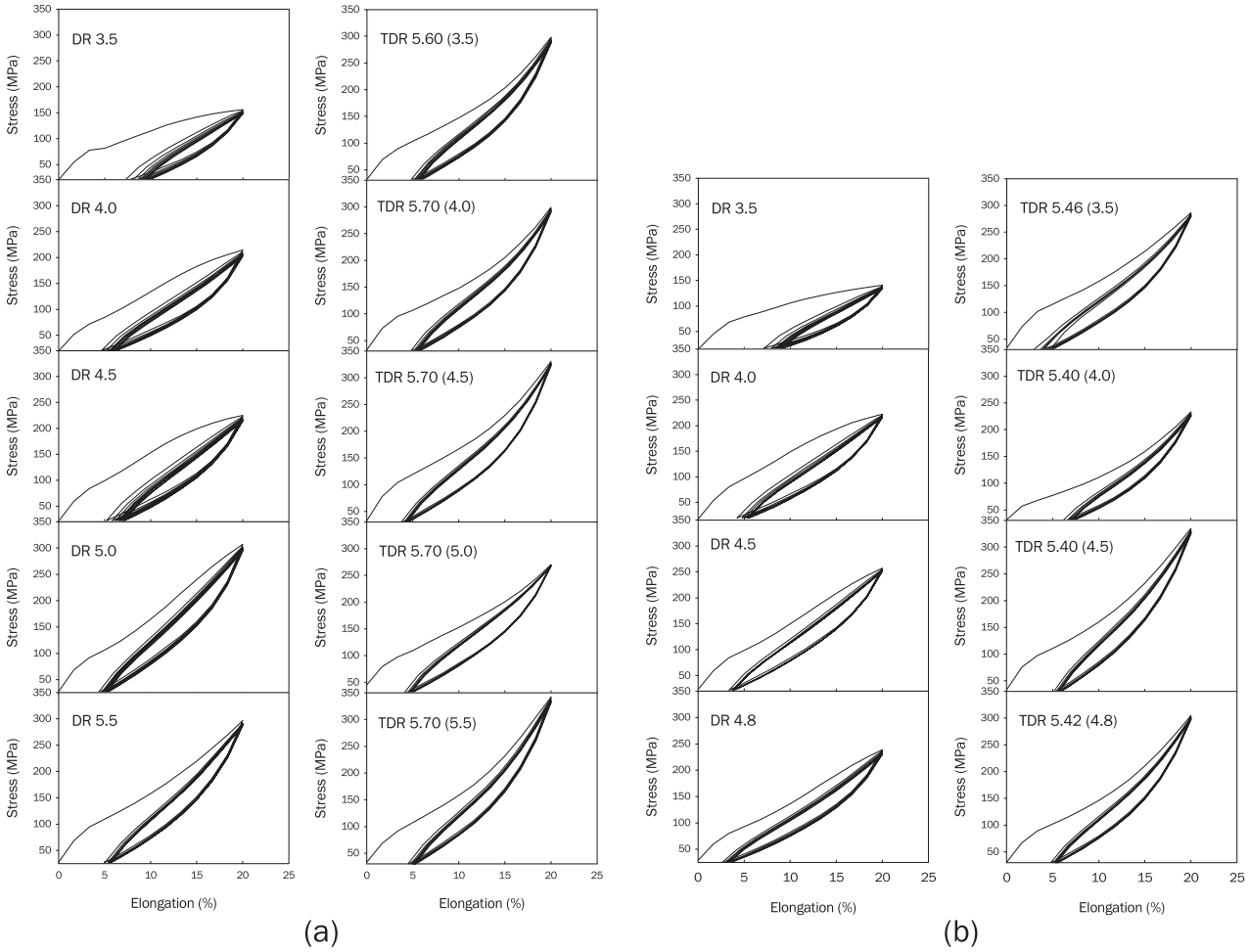

Fig. 11 Elastic recovery of bio- (a) and chemo-based (b) drawn PTT fiber. Draw ratios were noted inside figures.

Table 4 Mechanical properties for drawn PTT fibers.

Polymer types	Drawings	Draw ratio /Total draw ratio	Elastic recovery (%)		
			The first cycle	The fifth cycle	The tenth cycle
Bio-based PTT	The 1st drawing	3.5	93.0	91.2	90.6
		4.0	95.4	94.4	93.8
		4.5	94.8	93.4	92.8
		5.0	95.7	95.0	94.8
		5.5	95.0	94.4	94.3
	The 2nd drawing	5.60 (3.5)	95.4	94.7	94.5
		5.70 (4.0)	95.3	94.6	94.5
		5.70 (4.5)	96.3	95.8	95.7
		5.70 (5.0)	96.0	95.4	95.4
		5.70 (5.5)	95.6	95.0	94.9
Chemo-based	The 1st drawing	3.5	92.9	91.4	90.9
		4.0	95.8	94.7	94.5
		4.5	96.6	96.2	96.2
		4.8	97.5	96.8	96.6
	The 2nd drawing	5.46 (3.5)	97.3	94.6	94.4
		5.40 (4.0)	94.1	93.2	93.3
		5.40 (4.5)	95.0	94.5	94.5
		5.42 (4.8)	95.4	94.8	94.8

* Values in bracket beside total draw ratio are draw ratio of the first-step drawing.

the area in the center of a hysteresis loop indicates the energy dissipated due to material plasticity is slight. With increasing cycle count, the elastic recovery decreases, i.e. the latent elongation increases. Also the remnant elongation increases with draw ratio and by the second drawing. Elastic recoveries immediately after the first, fifth, and tenth cycles are presented in Table 4. The elastic recoveries attains above 90% under all conditions applied in this study. The PTT fibers obtained by the two-steps drawing show a good elastic recovery.

4. Conclusions

As-spun bio- and chemo-based PTT fibers of approximately 100 μm were drawn to draw ratios of 3.5-5.5 and 3.5-4.8 by the first drawing, i.e., CO_2 laser-heated neck-drawing, and to total draw ratios of 5.60-5.70 and 5.40-5.46 by the second drawing, i.e., direct contact heater drawing. The bio-based PTT fiber was steadily drawn to higher draw ratio with higher drawing stress than of the chemo-based one. On the other hand, by the two-steps drawing, the birefringence was the constant value 0.07, being over twice the reported intrinsic birefringence 0.029, The low intrinsic birefringence value is caused by the methylene chain conformation, trans-gauche-gauche-trans, of PTT chain in crystal. On the other hand, the amorphous molecular chains not only oriented along the fiber axis but also extended more linearly than the chain in the crystal as draw ratio increases. Eventually, the mechanical property increase with draw ratio by two-steps drawing, which is supported by the increase of amorphous orientation. Young's modulus held almost constant value of 2.3-2.6 GPa with no dependence on draw ratio of the two stages drawing, being very close to 2.59 GPa [5], the theoretical modulus of PTT crystal. Tensile strength noted the maximum value of 683 MPa (5.1cN/dtex) for bio-based fiber by the two stages drawing, and the elongation kept over 40% for the fiber. It is a noteworthy that the high-toughness PTT fiber which has both over 5 cN/dtex strength and over 40% elongation can be made by laser-heated drawing in this study. The stretch cycles to the elongation of 20% showed slight hysteresis loops, and the elastic recovery reached higher than 90% under all drawing conditions in this study.

Acknowledgement

This work was supported by the National Research Foundation of Korea Grant funded by the Korean Government (Ministry of Education, Science and Technology). [NRF-2010-359-D00031]

References

1. US Patent 20080176957A1.
2. R. Jakeways, I. M. Ward, M. A. Wilding, I. J. Deborough, M. G. Pass, *J. Polym. Sci. Polym. Phys.*

Ed. **13**, 799 (1975).
3. I. M. Ward, M. A. Wilding, H. Brody, *J. Polym. Sci. Polym. Phys. Ed*. **14**, 263 (1976).
4. K. Nakamae, T. Nishio, K. Hata, F. Yakoyama, T. Matsumoto, *Zairyo* **35**, 1066 (1986).
5. I. Sakurada, K. Kani, *J. Polym. Sci. Part C,* **31**, 57 (1970).
6. S. Poulin-Dandurand, S. Perez, J. F. Revol, F. Brisse, *Polymer*, **20**, 419 (1979).
7. I. J. Deborough, I. H. Hall, J. Z. Neisser, *Polymer*, **20**, 545 (1979).
8. B. Wang, C. Y. Li, J. Hanzlicek, S. Z. D. Cheng, P. H. Geil, J. Grebowicz, R. M. Ho, *Polymer* **42**, 7171 (2001).
9. J. Yang, G. Sidoti, J. Liu, P. H. Geil, C. Y. Li, S. Z. D. Cheng, *Polymer*, **42**, 7181 (2001).
10. J. S. Grebowicz, H. Brown, H. H. Chuah, J. M. Olvera, A. Wasiak, P. Sajkiewicz, A. Ziabicki, *Polymer*, **42**, 7153 (2001).
11. M. Pyda, A. Boller, J. Grebowicz, H. H. Chuah, B. V. Lebedev, B. Wunderlich, *J. Polym. Sci. Polym. Phys.*, **36**, 2499 (1998).
12. H. H. Chuah, *J. Polym. Sci. Polym. Phys.,* **40**, 1513 (2002).
13. K. H. Kim, Y. A. Kang, T. Murata, S. Ikehata, Y. Ohkoshi, Y. Gotoh, M. Nagura, M. Koide, H. Urakawa, M. Kotera, *Polymer* **49**, 5705 (2008).
14. W. Okumura, T. Yamaguchi, Y. Ohkoshi, Y. Gotoh, M. Nagura, *Intern. Polym. Proc.*, **117**, 124 (2002).
15. J. H. Dumbleton, *J. Polym. Sci. Polym. Phys.*, **6**, 795 (1968).
16. G. Wu, H. Li, Y. Wu, J. A. Cuculo, *Polymer*, **43**, 4915 (2002).
17. K. H. Kim, H. H. Cho, H. Ito, K. Kikutani, *J. Polym. Sci. Polym. Phys.,* **46**, 847 (2008).
18. W. S. Lyoo, H. S. Lee, B. C. Ji, S. S. Han, K. Kang, S. S. Kim, J. H. Kim, J. S. Lee, T. W. Son, W. S. Yoon, *J. Appl. Polym. Sci.,* **81**, 3471 (2001).
19. JP 2005-179639A
20. JP 1999-107036A